Electronic Journal «Technical Acoustics»
http://www.ejta.org

2008, 12

Nima Sahba, Vahid Tavakoli*, Alireza Ahmadian,
Mohammad D. Abolhassani, Mohammad Fotouhi

Research center for Science and Technology in Medicine, Tehran, Iran

Hybrid local/global optical flow and spline multi-resolution analysis of myocardial motion in B-mode echocardiography images

Received 18.11.2007, published 06.05.2008

Since myocardial motion is directly related to cardiac vascular supply, it can be helpful in diagnosing the heart abnormalities. The most comprehensive and available imaging study of the cardiac function is B-Mode echocardiography. Diagnostic systems are expert dependent and motion is not clear in the B-mode echocardiography images and therefore many efforts are toward proposing new methods to measure the motion accurately. Most of the previous motion estimation methods suffer from shear, rotation and wide range of motions due to the complexity of the myocardial motion in B-Mode images. In order to increase the accuracy and robustness to shear, rotation and wide range of motions, a hybrid method based on a newly introduced algorithm called combined local global (CLG) optical flow in combination with multi-resolution spatiotemporal spline moments is proposed. The method achieves rotational error of 2.8 degrees per frame and amplitude error of 3.8 percent per frame. These results demonstrate a better efficiency with respect to other B-Mode echocardiography motion estimation techniques such as Lucas-Kanade, Horn-Schunck and spatiotemporal affine technique.

Key words: echocardiography, cardiac motion, combined local/global optical flow, spline multi-resolution, myocardial motion estimation, optical flow.

1. INTRODUCTION

Cardiovascular disorder is one of the leading causes of death in the modern societies. Many efforts are in favor of achieving efficient techniques of cardiac function evaluation, one of the most important of which is echocardiography [1].

The analysis of myocardial motion, in particular, provides an efficient means to evaluate the degree of ischemia and infarction (based on the induced akinesia, hypokinesia or dyskinesia). In clinical practice, the analysis mainly relies on visual inspection or manual measurements by experienced cardiologists. Nevertheless expert-based methods are subjective, tedious and time consuming, and suffer from considerable inter- and intra-observer variability [2].

*Corresponding author, e-mail: vtavakoli@razi.tums.ac.ir

1.1. B-mode echocardiography motion detection

There are several methods of myocardial motion detection such as marker tracking or optical flow. Optical flow techniques are categorized into two major groups:

1. Block matching
2. Gradient based optical flow techniques

1.1.1. Block matching

The main idea toward this type of motion estimation is the fact that each block of a frame moves toward a similar block in another frame if the time interval is small enough. General strategy is to move the basic block toward other blocks and compute the distance from the most similar block [3].

1.1.2. Gradient based optical flow methods

Gradient-based optical flow methods are based on the first or the second derivation of consecutive frames. They are categorized into two classes: local methods such as Lucas-Kanade and structure tensor approach of Bigun and global methods like Horn-Schunck and its optimized versions for discontinuity preservation. There are also some other algorithms that can not be categorized in any of these classes (Phase-based method Of Fleet and Jepson) [4, 5, 6, 7, 8, 9, 10]. Local methods yield robustness under noise while global methods are empirically very sensitive to noise but have 100% density flow fields and induce visually attractive motion arrows (especially Anandan). Newer approaches are a combination of both local and global methods like 3-D CLG (Three Dimensional Spatiotemporal combination of Local and Global) to overcome failures of each method without loosing their advantages [11, 12].

1.2. B-mode myocardial motion estimation

There are many methods for cardiac motion extraction such as feature correlation and finite element models, endocardial tracking or myocardial tracking [13].

Meunier et al. used block matching methods as a motion estimation technique to extract cardiac motion. These methods were based on comparing the neighboring blocks using several methods such as Mean Absolute Difference (MAD), Mean Square Error (MSE) or correlation [14].

However their algorithm was simple but necessity for more rapid techniques led to application of other strategies such as gradient optical flow methods (Lucas-Kanade, Horn-Schunck, spatiotemporal affine model). Lucas-Kanade method presumes gray scale constancy between two consecutive frames. Chuncke was the pioneer of using optical flow in B-mode myocardial motion estimation and used uniform kernels of different sizes to reduce noise effect. He demonstrated that uniform kernels of degree 11 are the best. The second group following Chuncke was Baraldi et al who used three famous optical flow motion estimation techniques (Lucas-Kanade, Horn and Schunk and Nagel). In combination with Gaussian spatial and temporal kernels of different variances, they performed an optimization on kernel size and achieved an admirable comparison

between angular and rotational error of each method. Their evaluation was performed on simulated echocardiography images; a series of transformed echocardiography images with known amount of shear, translation, rotation or mixed of them [15]. Motion detection methods were also used in 3-D ultrasonography images [16, 17].

In an attempt to overcome different ranges of motion, Suhling and Unser developed a novel motion estimation technique called spatiotemporal affine model (Suhling-Unser) based on a fine to coarse spline moment strategy. They evaluated their data on simulated echocardiography and synthetic rotational phantom and proved their superiority in accuracy regarding other methods (Lucas-Kanade and Horn Schunck) [18].

1.3. Moment implementation and spatiotemporal multi-resolution strategy

Motion transformation matrix of a series of images is a combination of translation, rotation and shear. Therefore, many motion estimation methods are based on moments (Zernike or spline) to achieve some degrees of invariance and robustness to shear. On the other hand, moment implementation is not all the story. Pixels have different motion vectors in each region of the frames i.e. each region of an image translates, rotates or shears in various sizes. To overcome this problem Suhling et al. invented a multiresolution strategy inspired from previously introduced multi-resolution motion estimation methods such as Black and Anandan in which coarse kernel are performed on the whole image and then finer kernels are implemented until a certain amount of error is reached [18]. Different spectrum of motion can be preserved better and escape from damping in large kernels.

1.4. Spline basis functions

Splines are a group of basis functions which are compact support and have many interesting mathematical properties which make them efficient to be used in many processing applications. They are constructed from an iterative convolution based on which their support and smoothness increase from a rectangle to a Gaussian asymptotically in infinity. Below is formulation to clear that [19]:

$$\beta^0(x) = \begin{cases} 1, -\frac{1}{2} < x < \frac{1}{2}, \\ 1/2, |x| = \frac{1}{2}, \\ 0, Otherwise, \end{cases}, \qquad (1)$$

$$\beta^n(x) = \beta^0 * \beta^0 * ... * \beta^0,$$

where β^n is B-spline of degree *n* and * indicates convolution operator.

In this paper we will first propose a brief introduction to motion estimation techniques and their advantages and disadvantages. After that a new algorithm is proposed which is based on

positive points of each motion detection method. We show that motion estimation is more robust based on spline moments. Finally implementation on 3 types of data which are simulated (with ground truth), synthetic (still with ground truth) and real B-mode echocardiography (no ground truth but completely tangible) are given.

2. METHODS AND MATERIALS

2.1. General properties of ultrasound motion estimation

It is noteworthy that all motion estimation techniques are application-dependant and B-mode echocardiography motion estimation itself is a special frame work which is completely different from well-known ground truth sequences. Echocardiography signal has a particular speckled texture that is derived from the primary tissue microstructure and motion detection is based on this primary pattern displacements. Our contribution in this paper is implementing a combined form of optical flow based on two previous famous motion estimations methods (Lucas-Kanade and Horn-Schunck) using image moments instead of primary image pixels. To do that, appropriate window sizes and moment orders and sizes were obtained. As will be discussed penalizing functions are also justified on B-mode echocardiography image discontinuities.

2.2. Gradient based methods

2.2.1. Global constant motion (Horn and Schunck)

The general differential formulation of optical flow computation consists of assuming that the intensity of a particular point in a moving pattern does not change with time. This constant intensity assumption is written as:

$$\iint [(E_x u + E_y v + E_t)^2 + \alpha^2 (\|\nabla u\|^2 + \|\nabla v\|^2)] dx dy , \quad (2)$$

where E is pixel intensity with gradients toward spatial and temporal dimensions of the image, u and v is the motion vectors toward x and y directions and α is a weighting parameter [20, 21, 22]. However primary global methods have visually attractive motion fields but lack the discontinuity preservation property.

2.2.2. Locally constant motion (Lucas-Kanade)

To overcome the sub-dimensionality of the OF formulation in Equation (2), Lucas-Kanade proposed equation (3) to solve the problem on small local windows where the motion vector is assumed to be constant. We ought to minimize this equation:

$$\sum W^2(x)[E_x u + E_y v + E_t]^2 , \quad (3)$$

where E is pixel intensity, W is a weighted window and u and v are the motion vectors toward x and y directions [23].

Optical flow algorithms are based on the brightness constancy in an image and disruption of consecutive frames can be corruptive for any motion estimation [22, 24].

2.2.3. Spatiotemporal affine model

Inspired from Lucas-Kanade, Suhling et al. proposed an algorithm to combine affine information with the brightness constancy assumption. For further details on this approach, readers are referred to (Suhling et al., 2005).

$$\begin{bmatrix} s_1(x,t) \\ s_2(x,t) \end{bmatrix} = \begin{bmatrix} s_1^0 \\ s_2^0 \end{bmatrix} + \begin{bmatrix} s_{1x} & s_{1y} & s_{1t} \\ s_{2x} & s_{2y} & s_{2t} \end{bmatrix} . \begin{bmatrix} x - x^0 \\ y - y^0 \\ t - t^0 \end{bmatrix}, \tag{4}$$

where s_1 and s_2 are the affine vector in x, y and t directions [18].

2.2.4. 3-D combined local global

As discussed before, to solve the problem of sensitivity to noise, Bruhn et al. proposed a method to combine local Lucas-Kanade with global Horn-Schunck. To give a combined local-global method let us reformulate the previous formulae:

$$w = (u, v, 1)^T \Rightarrow |\nabla w|^2 = |\nabla u|^2 + |\nabla v|^2, \tag{5}$$

where w is the spatiotemporal motion vector.

It is evident that Lucas-Kanade minimizes the quadratic form:

$$\mathrm{E}_{\mathrm{LK}} = K_\rho (f_x + f_y + f_t)^2 = \begin{vmatrix} u \\ v \\ 1 \end{vmatrix} . \begin{vmatrix} f_x^{\,2} & f_x f_y & f_x f_t \\ f_y f_x & f_y^{\,2} & f_y f_t \\ f_x f_t & f_y f_t & f_t^{\,2} \end{vmatrix} . \begin{vmatrix} u & v & 1 \end{vmatrix} = w^T J_\rho (\nabla_3 f) w, \tag{6}$$

where K_ρ is the local kernel (usually a Gaussian), E_{LK} is the energy function of Lucas-Kanade and f_x, f_y, f_t denote the image intensity gradient with respect to Cartesian and temporal dimensions.

We have a similar formulation for Horn and Schunck with an iterative recursion:

$$E_{HS}(w) = \int_\Omega (w^T J_0 (\nabla_3 f) w + \alpha |\nabla w|^2) dx dy, \tag{7}$$

where E is the energy function of HS (Horn-Schunck), J is the motion tensor and w is the motion vector [11, 12, 25].

Then we can rewrite:

$$\nabla_3 f = (f_x, f_y, f_t)^T \Rightarrow J_p (\nabla_3 f) = K_\rho * (\nabla_3 f . \nabla_3 f^T). \tag{8}$$

By replacing the structure tensor $J_0(\nabla_3 f)$ instead of matrix $J_\rho(\nabla_3 f)$, we will have:

$$\Delta u - \frac{1}{\alpha} (f_x^{\,2} u + f_x f_y v + f_y f_t)^2 = 0, \tag{9}$$

$$\Delta u - \frac{1}{\alpha} (f_x f_y u + f_y^{\,2} v + f_y f_t)^2 = 0. \tag{10}$$

Its minimization induces below equation which satisfies Euler-Lagrange formula:

$$\begin{aligned}\Delta u-\frac{1}{\alpha}(k_\rho(f_x{}^2)u+k_\rho(f_x f_y)v+k_\rho(f_x f_t))=0,\\ \Delta v-\frac{1}{\alpha}(k_\rho(f_x f_y)u+k_\rho(f_y^2)v+k_\rho(f_y f_t)=0.\end{aligned} \tag{11}$$

Spatiotemporal approach is defined as:

$$E_{CLG}(w)=\int_\Omega(w^T J_\rho(\nabla_3 f)w+\alpha\left|\nabla w\right|^2)dxdy. \tag{12}$$

It is proved that non-quadratic (nonlinear) functions can preserve discontinuities better than quadratic functions (blurring in edges of an image in HS methods are due to quadratic smoothing). Inserting a non-quadratic penalizer will lead to:

$$E_{CLGNonquadratic}(w)=\int_\Omega(\Psi_1(w^T J_\rho(\nabla_3 f)w)+\alpha\Psi_2\left|\nabla_3 w\right|^2)dxdydt, \tag{13}$$

where Ψ_1 and Ψ_2 are the penalizers.

Therefore based on Lagrange equations, we have:

$$0=\sum_{j\in N(i)}\frac{u_i-u_j}{h^2}-\frac{1}{\alpha}(J_{11i}u_i+J_{12i}v_i+J_{13i}), \tag{14}$$

$$0=\sum_{j\in N(i)}\frac{v_i-v_j}{h^2}-\frac{1}{\alpha}(J_{21i}u_i+J_{22i}v_i+J_{23i}), \tag{15}$$

$$0=\sum_{j\in N(i)}\frac{\Psi'_{2i}+\Psi'_{2j}}{2}\frac{u_i-u_j}{h^2}-\frac{\Psi'_{1i}}{\alpha}(J_{21i}u_i+J_{22i}v_i+J_{23i}) \tag{16}$$

After a simple calculation, the iterative formulations in (25) and (26) are resulted.

$$u_i^{k+1}=(1-\omega)u_i^k+\omega\frac{\sum_{j\in N^-(i)}u_j^{k+1}+\sum_{j\in N^+(i)}u_j^k-\frac{h^2}{\alpha}(J_{12i}v^k{}_i+J_{13i})}{\left|N(i)\right|+\frac{h^2}{\alpha}J_{11i}}, \tag{17}$$

$$v_i^{k+1}=(1-\omega)v_i^k+\omega\frac{\sum_{j\in N^-(i)}v_j^{k+1}+\sum_{j\in N^+(i)}v_j^k-\frac{h^2}{\alpha}(J_{21i}u^{k+1}{}_i+J_{23i})}{\left|N(i)\right|+\frac{h^2}{\alpha}J_{22i}}, \tag{18}$$

where $N^-(i)=\{j\in N(i)\mid j<i\}$, $N^+(i)=\{j\in N(i)\mid j>i\}$, $N(i)$ is the neighborhood pixel region for implementing Gaussian-Seidel iteration. Indices i and j determine the backward and forward Gaussian-Seidel iterative pixels and k defines the iteration number [11, 12, 26].

2.3. Multi-resolution spatiotemporal coarse to fine approach

B-mode echocardiography images can be viewed as 2-D slices of a 3-D structure that may escape from the transducer field of view or enter from one slice to another slice (out of plane error). On the other side B-mode frames suffer from severe expansion or contraction and shear. So it is crucial to perform an invariant pattern based on spline moments. Moments have a hypergeometric structure achieving invariance with respect to time and space. This property protects the primary image from being distorted during the motion. Each part of myocardium has different motion amplitudes so it seems necessary to apply an adaptive moment size in a coarse to fine manner. This enables the algorithm in detecting wide range of motions more accurately. It has been proved that the spatiotemporal moment approaches are much more efficient especially in cardiac motion estimation. We implemented Spline moments of size 3 to 5 to achieve invariance and guaranty well posedness. Spline moments can be obtained based on transforming each spline basis function into the hypergeometric state as defined below:

$$m_{p,q,r}(x_0,y_0,t_0)=\int_{R^3} w(x-x_0,y-y_0,t-t_0)\,f(x,y,t)(x-x_0)^p(y-y_0)^q(t-t_0)^r\,dxdydt, \tag{20}$$

where $m_{p,q,r}$ is the corresponding moment filter of degrees p, q and r, f is the basis function and x, y and t directions denote Cartesian and time axes [18, 19, 24, 26].

2.4. Simulated B-mode echocardiography

One of the most important sequences to be used in the evaluation in this field is simulated B-mode echocardiography sequences.

Design of simulated dynamic B-mode echocardiography was performed as Baraldi et al. had done. This could model B-mode echocardiography not only in pattern and noise probabilistic but also in motion vectors (cardiac contraction and relaxation). We implemented simulation not only in 2-D four chamber images but also two chamber series (SAX and LAX). Even pathologic states were considered to cover various states of motions.

A circular cardiac model with periodic inward and outward flexion and deflexion was used to model a beating heart. This is performed by applying a radial displacement field with a magnitude decreasing with the distance from the center. This displacement field is cosine modulated in time to simulate the expansion and contraction. This kind of motion reflects the wall thinning and thickening of a beating heart during diastole and systole. The model presumes that the system forming the image has a linear and space invariant point spread function (PSF). If the biological tissue is modeled by a continuous distribution of point scatterers, whose impulse response is $T(x,y)$, then the radio-frequency image $I(x,y)$ can be obtained by spatial convolution of them:

$$I(x,y)=PSF\,(x,y)\otimes T(x,y), \tag{21}$$

$$PSF\,(x,y)=\cos\left(\frac{2\pi}{\lambda}\right)\exp\left(-\left(\frac{x^2}{\sigma_x^2}+\frac{y^2}{\sigma_y^2}\right)\right). \tag{22}$$

In particular, the *PSF* (Point Spread Function) was defined in terms of the acoustic wavelength (λ), standard deviation (σ) and the axial and lateral resolution of the imaging system as equation (30): [15, 28, 29].

We inserted transducer frequency 4 MHz, sound velocity 1540 m/s, wavelength 0.385 mm, spatial frequency of sound 5.195 cycles/mm, standard deviations (σ) along x and y axis 0.426 mm, standard deviation along z axis 0.213 mm, x and y axis range –5 to 5 mm, z axis range 0 to 5 mm. The pattern was added to the mobile circular or multi chamber cardiac model.

2.5. Synthetic phantom images

Suhling et al. performed cardiac motion estimation technique in a rotating phantom made of gelatin agar-agar. Angular velocity for their synthetic phantom was 0.0798 rps. However this is a good real approach that faces toward actual speckle motions in an image, it lacks the real texture of heart as a combination of myocardium and connective tissue. We synthesized a circular finely cut myocardial biopsy from a real post mortem human heart after fixation in the paraffin. The biopsy was carefully taken from the anterior wall of left ventricular myocardium. Its angular velocity was also 0.0798 rps in a tank of normal saline (150 meq/lit sodium chloride in sterile water) using a Siemens ultrasonography framework in the range of 7 MHz [18].

3. RESULTS

3.1. Implementation on simulated B-mode echocardiography

Simulated echocardiography has the most reliable ground truth for cardiac motion estimation and is based on ultrasound modeling of scatterers as discussed in 2.6.

A quantitative analysis of the performance of the algorithm was performed on simulated sequences for which the exact motion field is known. Previous studies only modeled short axis view of the heart only covering few abnormalities but here we try to cover all possible cardiac views in many normal and abnormal conditions.

All the methods in table 2 were implemented on simulated B-mode echocardiography frames and angular and amplitude errors were obtained using the popular equations mentioned in (23) and (24) [15, 18]:

$$amplitude \quad Error = \left| \frac{\left\| \hat{V} \right\| - \left\| V \right\|}{\left\| V \right\|} \right| .100 , \tag{23}$$

$$\theta_E = \arccos \frac{\left\langle V, \hat{V} \right\rangle}{\left\| V \right\| . \left\| \hat{V} \right\|} , \tag{24}$$

where θ_E is the angular error V and $\hat{V}$ define real and estimated vectors.

Spline basis function were generated and converted to hyper-geometric moments. Spline moments were performed from coarse to fine resolutions until a certain error was satisfied. Figure 1 shows 6 Spline basis functions while figure 2 illustrates a coarse and fine moment visually [19].

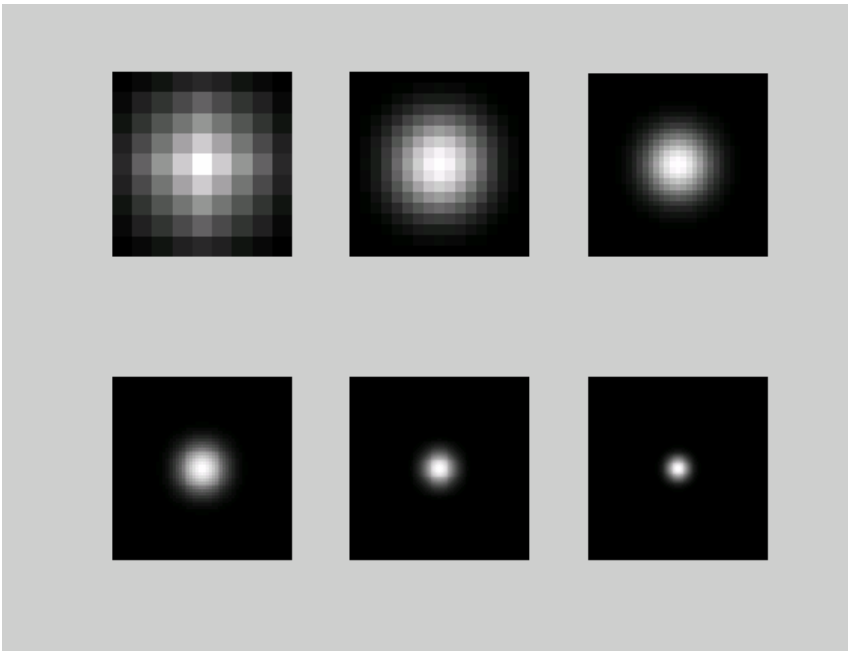

Figure 1. Spline basis functions: pictures define spline basis functions of degree 2, 3, 4, 5, 6, 7 respectively

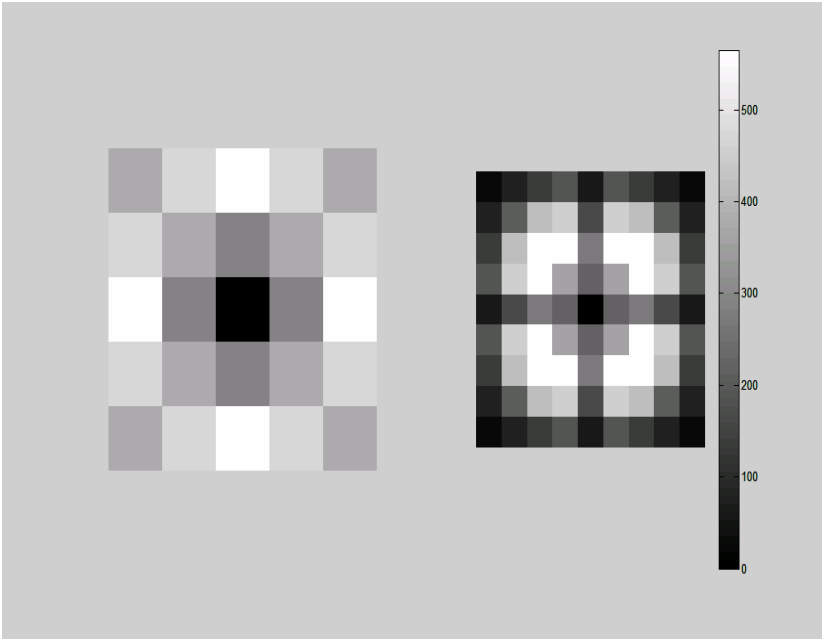

Figure 2. The left picture indicates a fine spline moment of size 5 and the right picture is a coarse spline of size 9

Methods were performed on the simulated echocardiography images through which angular and magnitude errors were extracted (table [1]). An optimization on alpha gave 2000 as the best one for computing CLG method. All applications were done on MATLAB 7.1, Intel processor 3 GHz and RAM 2048 MHz.

Table 1. Comparison between different speckle tracking methods

Method	Rotational Error (Degrees/frame)	Variance of rotational error (Degrees/frame)	Amplitude Error (percentile/frame)	Variance of amplitude error (percentile/frame)	Temporal burden (in seconds)
Lucas-Kanade	8.2	4	10.2	6.8	1.03
Suhling-Unser Spatiotemporal affine model	5	2.2	6.2	4.4	5.3
Horn and Shunke (15)	9	3.6	10.4	6.2	0.8
Horn and Shunke (75)	7.5	3.2	10.2	5	1.1
Horn and Shunke (125)	8	3.9	10.3	5.9	1.3
Hybrid 2-D CLG	4.6	2.1	3.9	1.5	1.8
Hybrid 3-D CLG	2.8	1.5	3.8	1.2	2.2
3-D CLG with 3 iterations (Warping)	1.4	0.9	2.2	1.1	30

Figures 3 and 4 illustrate the robustness of four famous motion detection techniques and superiority of the proposed approach with respect to variable amount of noise. Figure 5 shows one frame of the B-mode echocardiography simulation in addition to motion vectors.

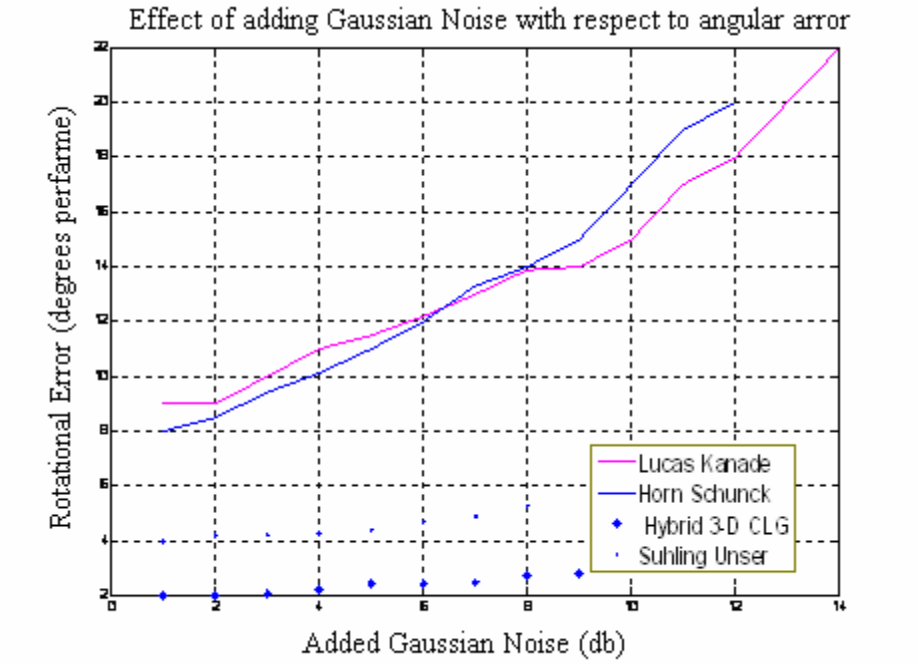

Figure 3. Robustness of angular accuracy of different motion estimation systems to noise

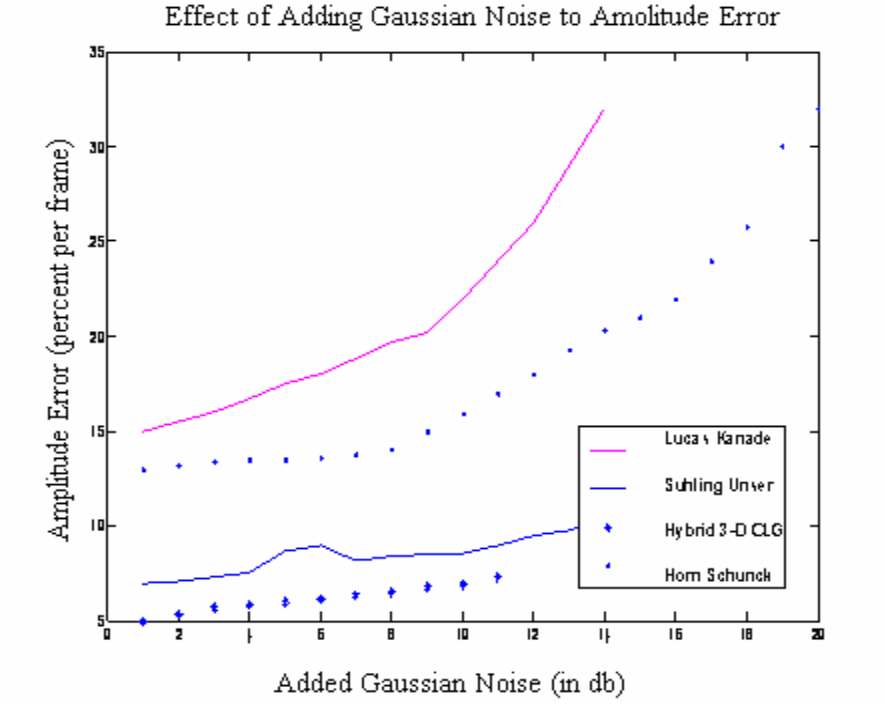

Figure 4. Robustness of amplitude accuracy of different motion estimation systems to noise

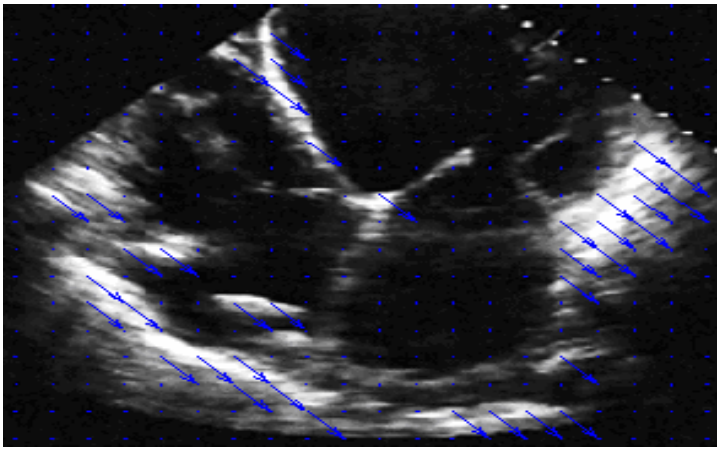

Figure 5. Simulated four chamber B-mode echocardiography (motion vectors are visualized as blue arrows) using 3-D hybrid CLG

3.2. Implementation on B-mode synthetic phantom images

While synthetic phantoms have a rotational motion around its center, it can well cover a large range of velocities. The farer we are from the center the higher the velocity is. Table 2 illustrates different velocities in different radii and its rotational and amplitude error. In the same way all algorithms were performed on synthetic data, whose results are depicted in the following table showing angular error, amplitude error and kernel efficiency. Table 2 illustrates the relative velocity errors in its corresponding radius (by increasing the radius, the velocity also increases) Figure 6 shows the result of the implementation of the proposed method on synthetic B-mode images.

Table 2. Comparison between results of LK (Lucas-Kanade), SU (Suhling-Unser) and hybrid 3-D CLG (Compare average error and its deviation in bold and normal columns respectively. Hybrid method seems to be the most accurate)

Radius (cm)	Velocity (cm/s)	**LK average error (cm/s)**	LK standard dev. (cm/s)	**SU multi-resolution average error (cm/s)**	SU multi-resolution standard dev. (cm/s)	**3D- hybrid CLG Average error(cm/s)**	3-D hybrid CLG Standard deviation (cm/s)
0.5	0.2	**0.02**	0.04	**0.01**	0.02	**0.01**	0.01
1	0.4	**0.032**	0.08	**0.02**	0.04	**0.015**	0.04
2	0.8	**0.042**	0.1	**0.02**	0.05	**0.018**	0.05
4	1.6	**0.094**	0.12	**0.06**	0.08	**0.035**	0.07
6	2.4	**0.14**	0.3	**0.12**	0.1	**0.1**	0.09
10	4	**0.24**	0.5	**0.2**	0.2	**0.1**	0.1
15	6	**0.6**	1.2	**0.45**	0.5	**0.21**	0.25
20	8	**1**	2.1	**0.68**	1	**0.32**	0.31
25	10	**1.3**	3.1	**0.89**	2	**0.39**	0.52

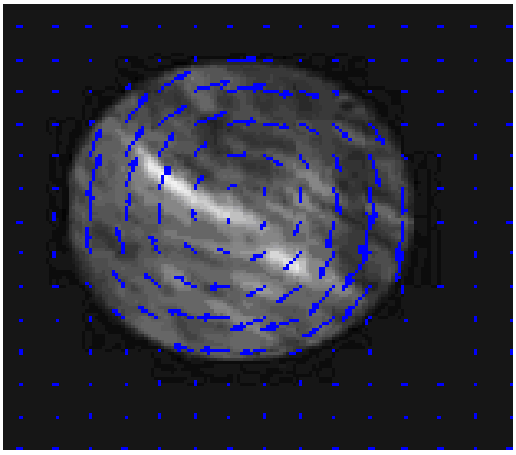

Figure 6.

Results of implementation of 3-D hybrid CLG method on rotating phantom images after adding 10 db white Gaussian noise

3.3. Floating centroid in real B-mode images

A very helpful feature for cardiologists in computerized B-mode velocity estimation is extracting a centroid regarding which all other motions are calculated proportionally. This implementation is simplistic in an engineering view but is of great importance for a physician. Using this correction technique, clinicians are able to differentiate global translation of human heart from local motions and discern differences between two parallel walls which are moving in the same direction but with different velocities.

3.4. Implementation on the real human B-mode echocardiography data

Figures 7, 8 and 9 show the implementation of Lucas-Kanade, Horn-Schunck and the proposed technique on real B-mode echocardiography images respectively. It is clinically evident that the proposed technique can achieve better results. However we can not easily have a ground truth for real human cardiac motion, we can use clinically predictable situations. To approve our method clinically on actual data, we used echocardiography series of two patients who incidentally suffered from myocardial infarction and their cardiac muscle became dyskinetic (B-mode frames were prepared before and after infarction accidentally). Such cases could well model an in vivo acute downhill in myocardial function as dyskinetic, hypokinetic or akinetic points. Numerical studies showed 45% decrease in average myocardial motion amplitude after MI which indicates a general cardiac hypokinesia (figure 10). Figures 11 and 12 show the color-coded motion in real and simulated data with respect to the center point.

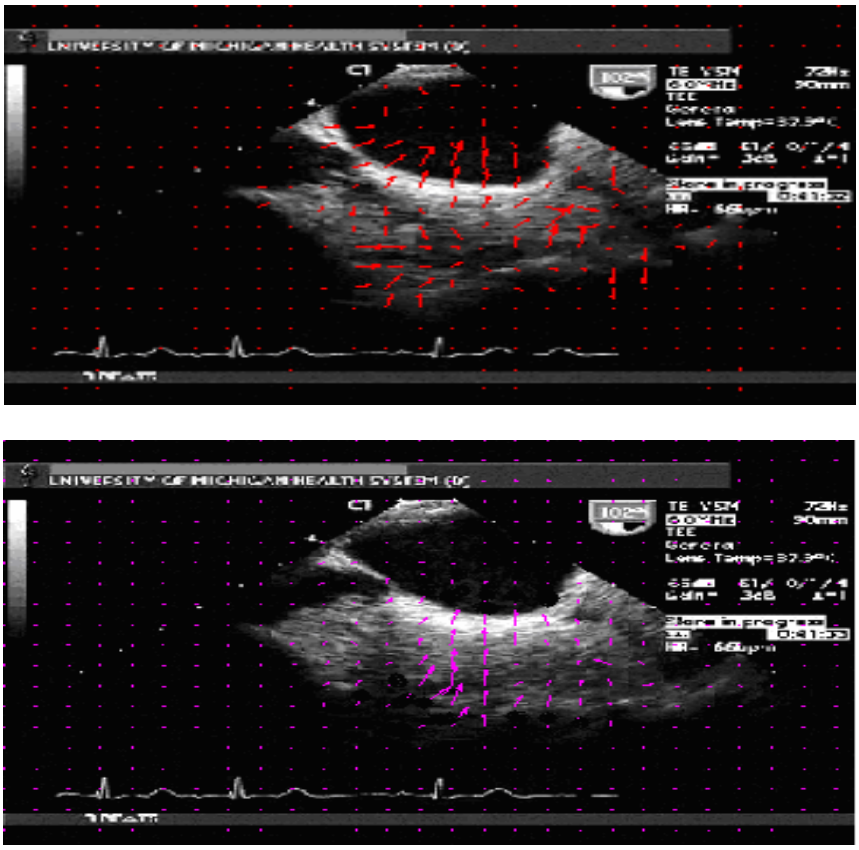

Figure 7. (a) Upper: Implementation of Lucas-Kanade on TEE, B-mode echocardiography images, (b) lower: implementation of the proposed method on the same sequence

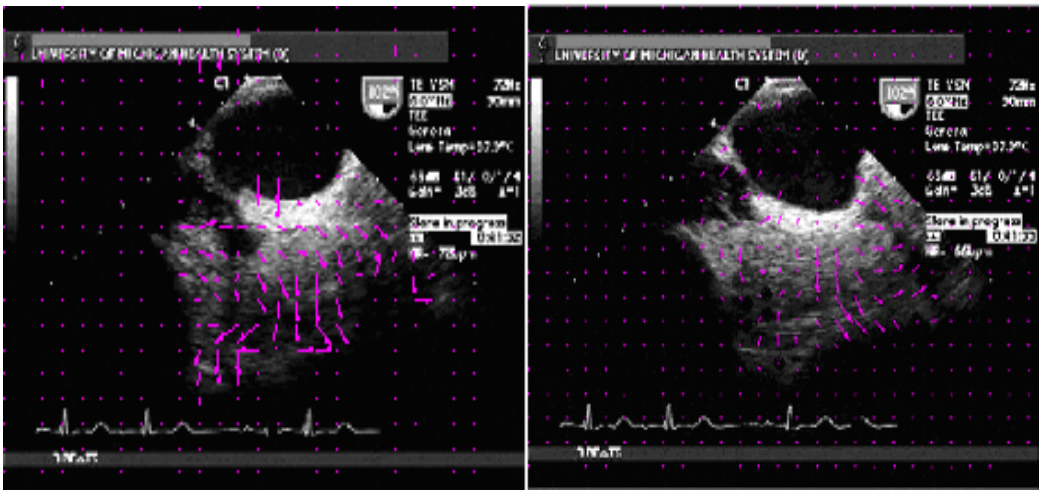

Figure 8. Implementation of Horn-Schunck (left) and the proposed method (right) on TEE, B-mode echocardiography

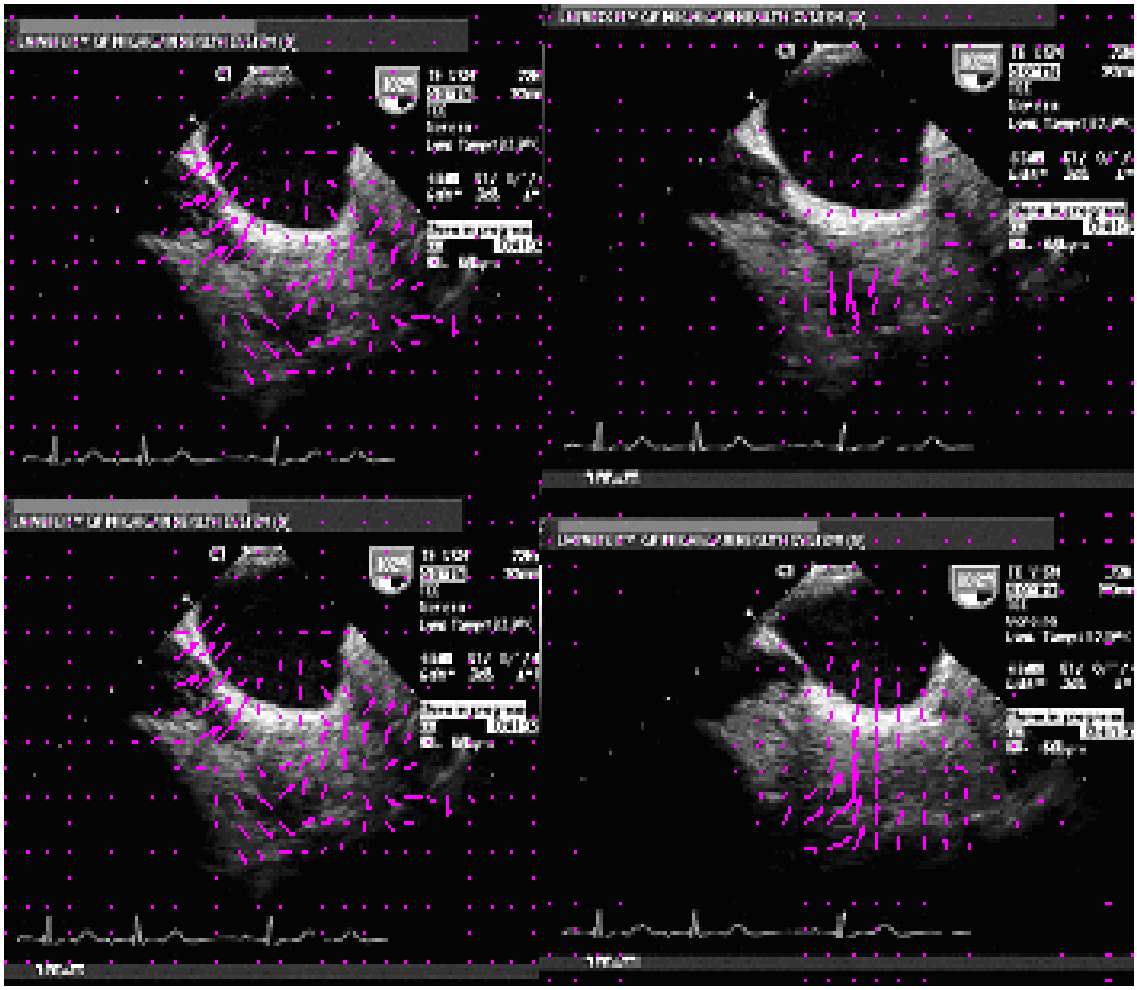

Figure 9. These frames are taken from the first of relaxation (diastole) in the left upper until end of contraction (systole) in right lower

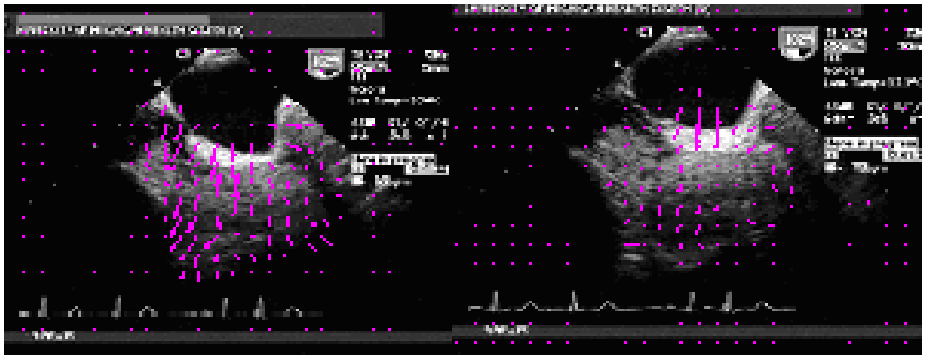

Figure 10. Myocardial motion estimation using 3-D CLG before (left) and after (right) MI. A general decrease in myocardial motion is evident in the ventricular myocardium

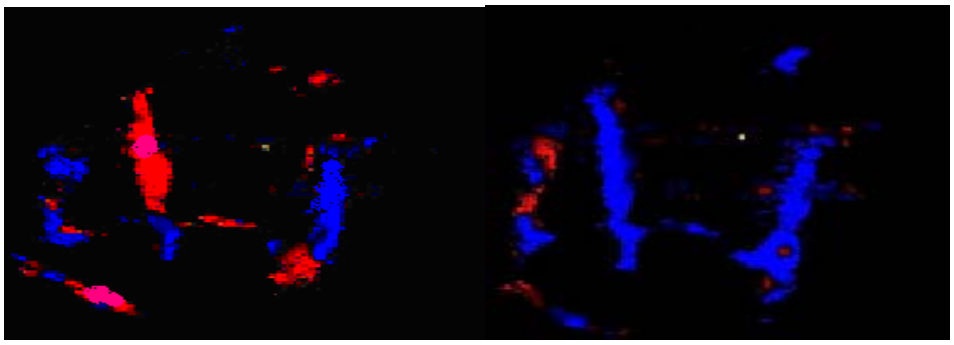

Figure 11.Color coded image illustrating the four chamber cardiac motion with respect to the central point (the yellow star). Notice the (right) image which was taken during systole and the (left) image taken during diastole

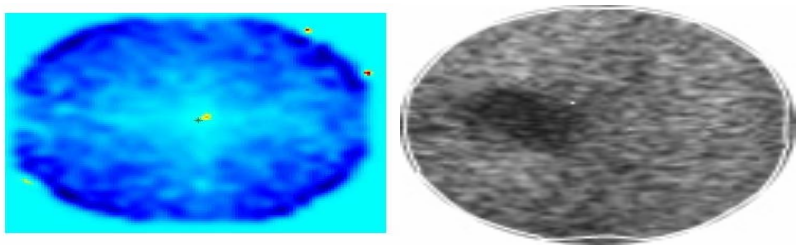

Figure 12. (Left) Color-coded result of implementation of 3-D CLG on simulated B-mode myocardial mass which is contracting toward the center with a velocity modulated in cosine function. Notice the green star in the center of the image. (Right) The primary image

CONCLUSION

We used 3-D CLG in combination with spline multi-resolution to overcome the noise and shear sensitivity of Horn-Schunck without loosing the benefits of a global method. It was shown that 3-D CLG can extract motion estimation vectors with rotational error of 2.8 degrees per frame and amplitude error of 3.8 percent. Visually attractive flow fields were obtained from B-mode echocardiography images. Experimental results showed correlation with clinical situations.

Implementation on simulated data showed the robustness of this method to even large amounts of noise. On the other side, implementation on the synthetic phantom sequence achieved a more real evaluation of efficiency of the proposed method. Moreover 3-D CLG based B-mode myocardial motion estimation could well correlate with the underlying clinical and physiological mechanics.

This paper is on the other side a good evaluation on optical flow techniques in the field of myocardial motion detection covering several gradient based algorithms.

We are currently working on motion segmentation based flow analysis and using full multi-grid and successive over relaxation to optimize the iterative methods and coarse to fine multi-resolution strategy.

REFERENCES

1. Leitman M. et al. Two-dimensional strain-novel software for real-time quantitative echocardiographic assessment of myocardial function. Journal of the American Society of Echocardiography, 2004, 17(2), 1021–1030.

2. Bohs L. N. et al. Speckle tracking for multidimensional flow estimation. Ultrasonics, 2000, 38(2), 369–375.

3. Abolhassani M. D., Norouzi A., Takavar A., Ghanaati H. Noninvasive temperature estimation using sonographic digital images. J. Ultrasound Med., 2007, 26(2), 215–222.

4. Alvarez L., Weickert J., Sanchez J. Reliable estimation of dense optical flow fields with large displacements. International Journal of Computer Vision, 2000, 39(1), 41–56.

5. Aubert G., Deriche R., Kornprobst P. Computing optical flow via variational techniques. SIAM Journal on Applied Mathematics, 1999, 60(1), 156–182.

6. Bigun J., Granlund G. H. Optical flow based on the inertia matrix in the frequency domain. In Proc. SSAB Symposium on Picture Processing, Lund, Sweden, 1988, 200–211.

7. Lamberti C. et al. Estimation of global parameters for the analysis of left ventricular motion. Presented at Computers in Cardiology, Rotterdam, The Netherlands, 2001, 429–432.

8. Bigun J., Granlund G. H., Wiklund J. Multidimensional orientation estimation with applications to texture analysis and optical flow. IEEE Transactions on Pattern Analysis and Machine Intelligence, 1991, 13(8), 775–790.

9. Black M. J., Anandan P. Robust dynamic motion estimation over time. In Proc. 1991 IEEE Computer Society Conference on Computer Vision and Pattern Recognition, IEEE Computer Society Press: Maui, HI, 1991, 292–302.

10. Nagel H.-H. Constraints for the estimation of displacement vector fields from image sequences. In Proc. Eighth International Joint Conference on Artificial Intelligence, vol. 2, Karlsruhe, West Germany, 1983, 945–951.

11. Bruhn A., Weickert J., Schnorr C. Combining the advantages of local and global optic flow methods. In Pattern Recognition of LNCS, Springer, 2002, 2444, 454–462.

12. Bruhn A., Weikert J, Schnorr C. Lucas-Kanade meets Horn and Schunk: combining local and global optic flow methods. Int. J. Comp. Vis., 2005, 61(3), 211–231.

13. Lin N., Papademetris X., Sinusas A. J., Duncan J. S. Analysis of left ventricular motion using a general robust point matching algorithm. In: Medical Image Computing and Computer-Assisted Intervention of LNCS, 2003, 1496, 556–563.

14. Weickert J., Schnorr C. A theoretical framework for convex regularizers in PDE-based computation of image motion. International Journal of Computer Vision, 2001, 45(3), 245–264.

15. Baraldi P. et al. Evaluation of differential optical flow techniques on Synthesized echo images. IEEE Transactions on Biomedical Engineering, 1996, 43(2), 259–272.

16. Lamberti C. et al. Topology of optical flowing 3D echocardiography. Presented at Computers in Cardiology, Lund, Sweden, 1997, 227–230.

17. Abolhassani A., Tavakoli V. Noninvasive thermal change detection in renal artery revascularization therapy. Submitted to Journal of Ultrasound in Medicine.

18. Suhling M., et al., Myocardial motion analysis from B-mode echocardiograms. IEEE Transaction on Image Processing, 2005, 14, 525–553.

19. Unser M. Splines: A perfect fit for signal and image processing. IEEE Signal Process. Mag., 1999, 16(6), 22–38.

20. Fleet D.J. and Jepson A.D. Computation of component image velocity from local phase information. International Journal of Computer Vision, 1990, 5(1), 77–104.

21. Galvin B., McCane B., Novins K., Mason D., Mills S. Recovering motion fields: An analysis of eight optical flow algorithms. In Proc. 1998 British Machine Vision Conference, Southampton, England, 1998.

22. Tavakoli V., Sahba N. et al. An evaluation of different optical flow techniques for myocardial motion analysis. IEEE proceeding on biomedical engineering, Kuala Lumpur, Malaysia, 2008.

23. Lucas B., Kanade T. An iterative image registration technique with an application to stereo vision. In Proc. Seventh International Joint Conference on Artificial Intelligence, Vancouver, Canada, 1981, 674–679.

24. Tavakoli V., Sahba N. et al. Adaptive multi-resolution myocardial motion analysis of B-Mode echocardiography images using Combined Local/Global optical flow. IEEE proceeding on Bioinformatics and Biomedical Engineering (iCBBE), Shanghai, China, 2008. (In press).

25. Bruhn A. Regularization in motion estimation. Master's thesis, Department of Mathematics and Computer Science, University of Mannheim, Germany, 2001.

26. Weickert J., Schnorr C. Variational optic flow computation with a spatiotemporal smoothness constraint. Journal of Mathematical Imaging and Vision, 2001, 14(3), 245–255.

27. Tavakoli V., Ahmadian A. et al. A new optical flow technique for myocardial motion analysis based on affine concept in space and time. Submitted to IEEE transaction on medical imaging.

28. Tavakoli V., Sahba N. et al. An Optimized two-stage method for ultrasound breast image compression. IEEE proceeding on biomedical engineering, Kuala Lumpur, Malaysia, 2008.

29. Meunier J. et al. Assessing local myocardial deformation from speckle tracking in echography. SPIE Med. Imag., 1988, 20–29.